Stress-based aftershock forecasts made within 24 hours post-mainshock: Expected north San Francisco Bay area seismicity changes after the 2014 *M*=6.0 American Canyon earthquake

Tom Parsons[1], Volkan Sevilgen[2], Margaret Segou[3], Kevin Milner[4], Edward Field[5], and Ross S. Stein[1]

Abstract. We calculate stress changes resulting from the *M*=6.0 American Canyon earthquake on north San Francisco Bay area faults. The earthquake ruptured within a series of long faults that pose significant hazard to the Bay area, and we are thus concerned with potential increases in the probability of a large earthquake through stress transfer. We conduct this exercise as a prospective test because the skill of stress-based aftershock forecasting methodology is inconclusive. We apply three methods: (1) generalized mapping of regional Coulomb stress change, stress changes resolved on Uniform California Earthquake Rupture Forecast (UCERF) faults, and a mapped rate/state aftershock forecast. All calculations were completed within 24 hours after the mainshock, and were made without benefit of known aftershocks, which will be used to evaluative the prospective forecast. All methods suggest that we should expect heightened seismicity on parts of the southern Rodgers Creek, northern Hayward, and Green Valley faults.

1. Introduction

On August 24 2014 the largest earthquake since the 1989 *M*=7.0 Loma Prieta shock struck the San Francisco Bay area, the *M*=6.0 American Canyon event. This earthquake nucleated ~11 km beneath Napa Valley on or near the West Napa fault, which is itself one a series of sub-parallel right-lateral strike-slip faults that comprise the San Andreas fault system. The *M*=6.0 earthquake injured 120 people, 3 critically, and caused localized damage in Napa Valley. The setting of this earthquake between the Hayward-Rodgers Creek system to the west, and the Concord-Green Valley faults to the east (Figures 1, 2), raises concerns that stress imparted by the

[1]U.S. Geological Survey, Menlo Park, CA
[2] Seismicity.net, San Carlos CA
[3]Geosciences Azur, France
[4] Southern California Earthquake Center, University of Southern California
[5]U.S. Geological Survey, Golden, CO

American Canyon earthquake might bring sections of these faults closer to failure, potentially triggering $M>7$ events [e.g., *Field et al.*, 2014]. We additionally want to test stress change forecasting prospectively by making calculations on the same day of the earthquake before seeing the spatial pattern of aftershocks. While there will be more refined information about the American Canyon earthquake rupture available in the future, our goal is to attempt to forecast immediate seismicity effects on surrounding faults at a variety of scales. As there is uncertainty about the most effective approach, we try a number of methods. We will revisit this prospective forecast in subsequent years to evaluate its performance based on subsequent seismicity, creep, and surface strain.

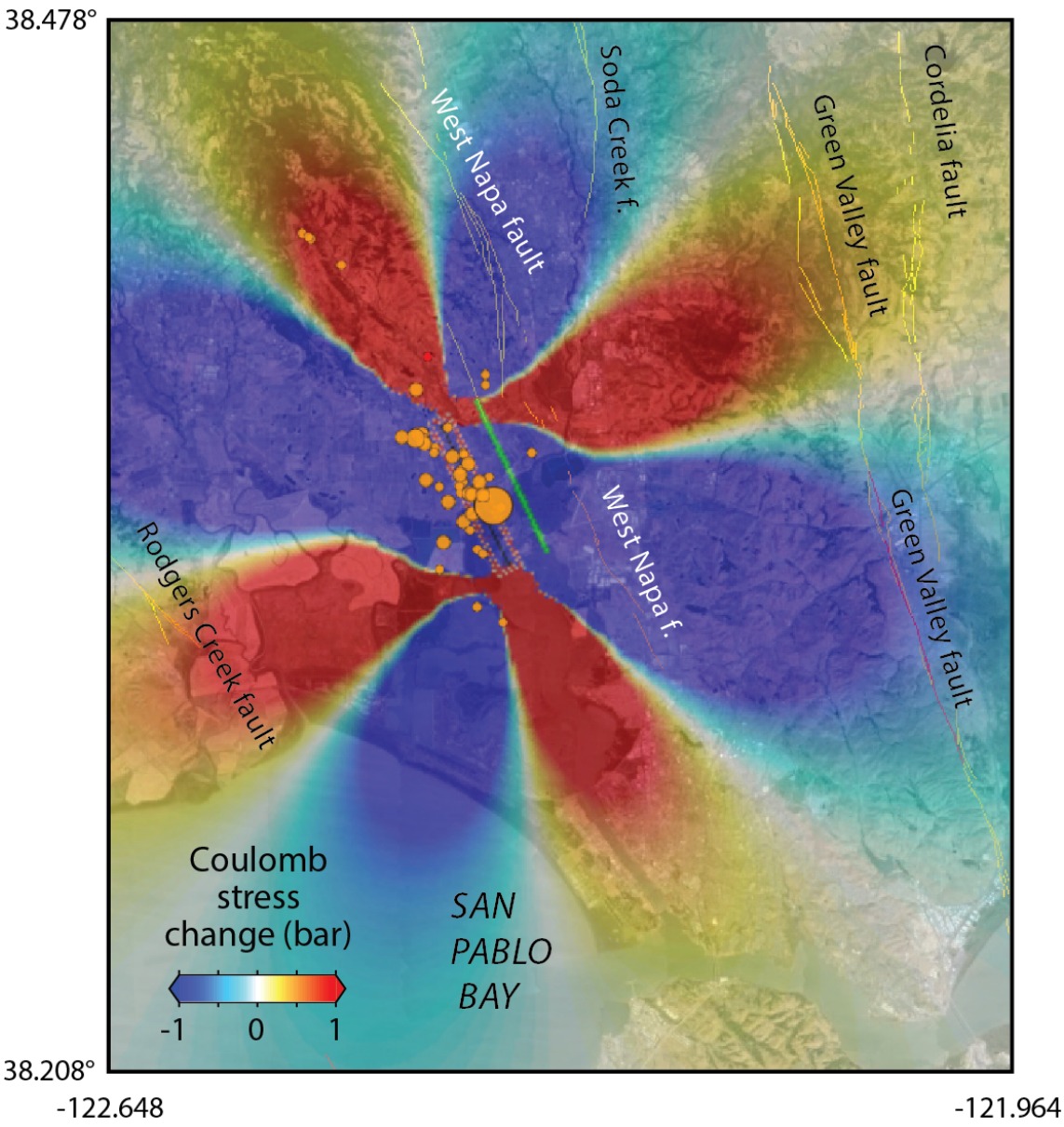

Figure 1. Coulomb stress change surrounding the American Canyon rupture; warm colors show calculated stress (and therefore, hazard) increase and cool colors show decreases (stress shadows). Based on the initial seismic moment and initial 4-hr of aftershocks, a 6 km x 6 km square source centered at 11 km depth with 1.3 m of slip was used to simulate the *M*=6.0 American Canyon earthquake; the surface projection of the rupture surface is shown as the dashed red rectangle; the rupture plane projects to the ground surface along the green line. The NCSS CMT solution with a 155° strike, 82° dip, and 172° rake, was used for the source. For simplicity, the same geometry is assumed for all receiver faults, as they are predominantly vertical and right-lateral, on which a friction coefficient of μ=0.4 was assumed. We calculate a ~0.25-bar stress increase on portions of the Green Valley and Rodgers Creek faults, and a ~0.75-bar stress decrease along most of the West Napa fault.

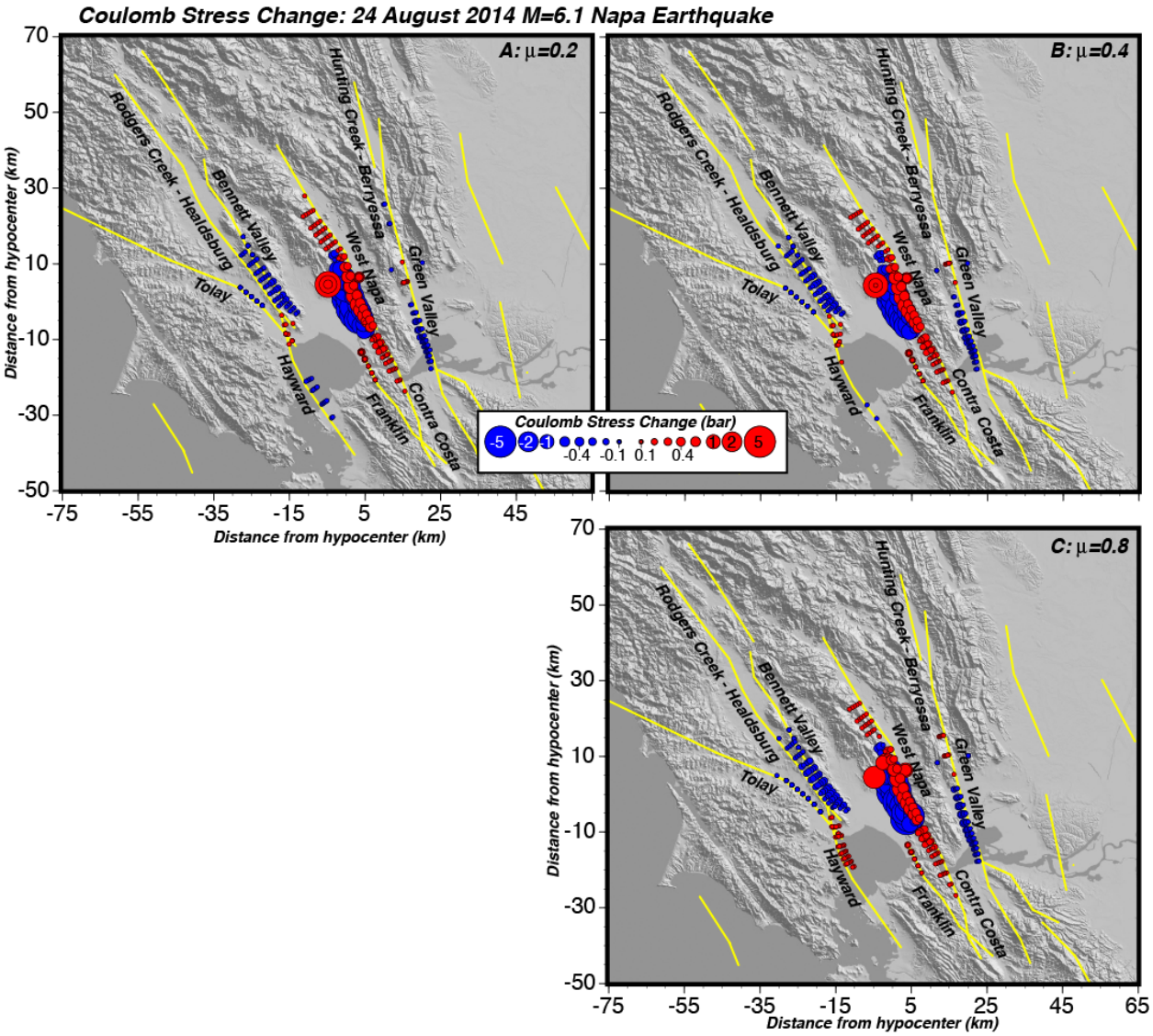

Figure 2. Coulomb stress change resolved on mapped faults defined by the Uniform California Earthquake Rupture Forecast Version 3 (UCERF3). Red dots correspond to calculated stress increases, whereas blue dots correspond to calculated decreases. Dots are located at centers of receiver fault patches (~3km x 3km); dipping faults are thus wider in map view. Regardless of friction coefficient used (a-c), we find that the Hayward-Rodgers Creek fault junction, the Franklin fault, the Contra Costa shear zone, and the West Napa fault have calculated stress increases.

2. Methods

We apply three different methods for stress-based aftershock forecasting, all of which were completed within 24 hours of the American Canyon earthquake. We intentionally do not incorporate any updated information available after the initial 24-hour period so that we can test rapid stress-based response methods. Parsons (Figure 2) and Segou (Figure 3) did not see the distribution of aftershocks before making their models; Sevilgen and Stein (Figure 1) used the first 4 hours of aftershocks to infer the rupture length. All calculations are made with preliminary information about the mainshock rupture, namely, the Northern California Seismic System (NCSS) centroid moment tensor (CMT) solution (http://www.ncedc.org/mt/nc72282711_MT.html), and could be readily automated for operational earthquake forecasting.

2.1 Coulomb stress change mapping on generalized fault planes

We calculate Coulomb stress change by simulating an earthquake with a slipping dislocation in an elastic half space [*Okada*, 1992; *Toda et al*. 1998; *Stein*, 1999] (Figure 1). Here a 6-km by 6-km square rupture source with geometry taken from the NCSS CMT solution (155° strike, 82° dip, 172° rake) with 1.3 m of slip centered at the hypocenter 11 km deep conserves the *M*=6.0 American Canyon earthquake moment (1.3 x10^{25} dyne-cm). The Coulomb criterion (*ΔCFF*) is defined by

$$\Delta CFF \equiv \left|\Delta\bar{\tau}_f\right| + \mu'(\Delta\sigma_n - \Delta p) \qquad (1)$$

where $\Delta\bar{\tau}_f$ is the change in shear stress on the receiver fault (set positive in the direction of fault slip), μ is the coefficient of friction, $\Delta\sigma_n$ is the change in normal stress acting on the target fault (set positive for unclamping), and Δp is pore pressure change. The Coulomb stress change is resolved on receiver fault planes that could have any geometry, rake, and friction. Here, the receivers are assumed to have the same characteristics as the rupture source, which is consistent with the regional northwest trending strike-slip tectonics of the San Andreas fault system. The calculation in Figure 1 assumes a receiver fault friction coefficient of μ =0.4, and pore fluid effects are neglected.

2.2 Coulomb stress resolved on mapped fault planes

An alternative approach to stress change calculation focuses on mapped faults. This technique is less likely to capture the complete spatial pattern of aftershocks, but appears to be effective at forecasting higher magnitude earthquakes [*Parsons et al.*, 2012]. We work with faults defined by the Uniform California Earthquake Rupture Forecast Version 3 (UCERF3) [*Dawson*, 2013], which have geometries and rakes determined through a geological consensus process, and have calculated earthquake rupture rates [*Field et al.*, 2014]. Receiver faults are divided up into ~3-km by ~3-km patches and Coulomb stress is resolved on each (Figure 2). The receiver fault friction coefficient is almost impossible to know even in detailed studies, so a range is used here from μ=0.2 to μ =0.8. We use the NCSS CMT solution parameters for the mainshock slip model modified slightly to match the UCERF3 geometry for the West Napa fault (155° strike, 75° dip, 180° rake). We centered the source dislocation at the initial reported hypocenter depth of 10.7 km, and scaled its dimensions using the regressions of *Wells and*

Coppersmith [1994] for strike-slip rupture length (16 km), width (7.7 km), and average slip (0.15m) at depth for a *M*=6.0 earthquake.

2.2.1 Interaction probability changes

We assess the impact of the American Canyon earthquake by calculating earthquake probability changes on major faults. A stress change can theoretically advance or delay earthquakes by time *T'*, which can be calculated by dividing the stress change (*ΔCFF*) by the tectonic stressing rate ($\dot{\tau}$), as $T'=\Delta\tau/\dot{\tau}$. Time-dependent probability calculations can be adjusted by accruing probability from the last earthquake time modified by the advance or delay (T_0+T'). Alternatively, the earthquake recurrence interval μ can be adjusted by the clock change as $\mu=\mu_0-T'$. We use the latter approach since the last earthquake time is unknown for north Bay Area faults.

To explain Omori-law transient earthquake rate changes with rate/state theory, *Dieterich* [1994] derived an expression for time-dependent seismicity rate *R(t)*, after a stress perturbation as

$$R(t)=\frac{r}{\left[\exp\left(\frac{-\Delta CFF}{a\sigma}\right)-1\right]\exp\left[\frac{-t}{t_a}\right]+1} \qquad (2)$$

where *r* is the steady-state seismicity rate, *ΔCFF* is the stress step, σ is the normal stress, *a* is a fault constitutive constant, and t_a is an observed or inferred aftershock duration. We assume t_a to be 10 years, and derive the $a\sigma$ parameter from $a\sigma=t_a\cdot\dot{\tau}$ [*Dieterich*, 1994], which yields values

between 0.25-0.5 bars based on loading rates from *Parsons* [2002], and is reasonably consistent with the 0.5 bar value of *Toda* [2005].

The transient earthquake rate $R(t)$ after a stress step can be related to earthquake probability over the interval Δt as

$$P(t,\Delta t) = 1 - \exp\left[-\int_t^{t+\Delta t} R(t)dt\right] = 1 - \exp(-N(t)), \tag{3}$$

[*Dieterich and Kilgore*, 1996], where $N(t)$ is the expected number of earthquakes in the interval. The transient probability change can be superimposed on recurrence interval change. Integrating for $N(t)$ yields

$$N(t) = r_p\left\{\Delta t + t_a \ln\left[\frac{1+\left[\exp\left(\frac{-\Delta CFF}{a\sigma}\right)-1\right]\exp\left[\frac{-\Delta t}{t_a}\right]}{\exp\left(\frac{-\Delta CFF}{a\sigma}\right)}\right]\right\} \tag{4}$$

where r_p is the expected rate of earthquakes associated with the permanent probability change [*Toda et al.*, 1998]. This rate can be determined by applying a stationary Poisson probability expression as

$$r_p = \left(\frac{-1}{\Delta t}\right)\ln\left(1 - P_c\right) \tag{5}$$

where P_c is a conditional probability, and can be calculated using any distribution. The time-dependent Brownian Passage Time model is used here [*Matthews et al.*, 2002], with a fixed aperiodicity of 0.5, and recurrence intervals from *Field et al.* [2014]. No dates of past large earthquakes are known for north San Francisco Bay region faults, so we use the method of *Field and Jordan* [2014] to account for unknown time of last event before an historical open interval (t_H=AD1776 for the San Francisco Bay region, *WGCEP* [2003]) as

$$P\left(\Delta t \middle| t > t_H\right) = \frac{\Delta t - \int_{t_H}^{t_H+\Delta t} F(t)\,dt}{\int_{t_H}^{\infty}\left[1 - F(t)\right]dt} \quad . \tag{6}$$

2.3 Coulomb and Rate/State aftershock forecasting

We lastly combine Coulomb stress changes and rate/state equations [*Dieterich*, 1994] to map expected seismicity rates following the stress perturbation from the American Canyon event. To model the evolution of seismicity, we calculate Coulomb stress change on a 2.5 km by 2.5 km grid at target depth 10 km imparted by the American Canyon earthquake for optimally-oriented planes (friction varying over μ=0.2 to μ =0.8), with a regional stress field representation taken from *Hardebeck and Michael* [2004], with the maximum compressive stress set to N19°E at a differential stress magnitude of σ1- σ3=10 MPa [*Toda et al.*, 2005]. We make a second calculation under an assumption that all receiver faults on the grid have properties akin to the Hayward fault (strike=N34˚W, dip=90˚, rake=180˚) (Figure 3a-b). We include uncertainty in receiver fault friction over a range of μ=0.2 to μ =0.8.

Under rate/state theory, a stress perturbation (*ΔCFF*) causes the state variable of the system γ_{n-1} before the event to evolve co-seismically to a new value γ_n,

$$\gamma_n = \gamma_{n-1} exp\left(\frac{-\Delta CFF}{a\sigma}\right) \quad (7)$$

The forecast seismicity rate *R* is then found from

$$R = \frac{r}{\gamma \dot{\tau}}. \quad (8)$$

This model depends on three parameters: (1) the reference seismicity rate *r* (background seismicity rate), which is taken from *M*≥3.0 rates during a 1974-2014.235 period, (2) the mean secular fault loading rate on all faults surrounding the rupture ($\dot{\tau}$ =0.05 bar/yr) [*Parsons*, 2002], and (3) the *aσ* term, taken to be 0.5 bar after *Toda et al.* [2005]. We estimate expected *M*≥3.0 seismicity at each node for the first week after the mainshock.

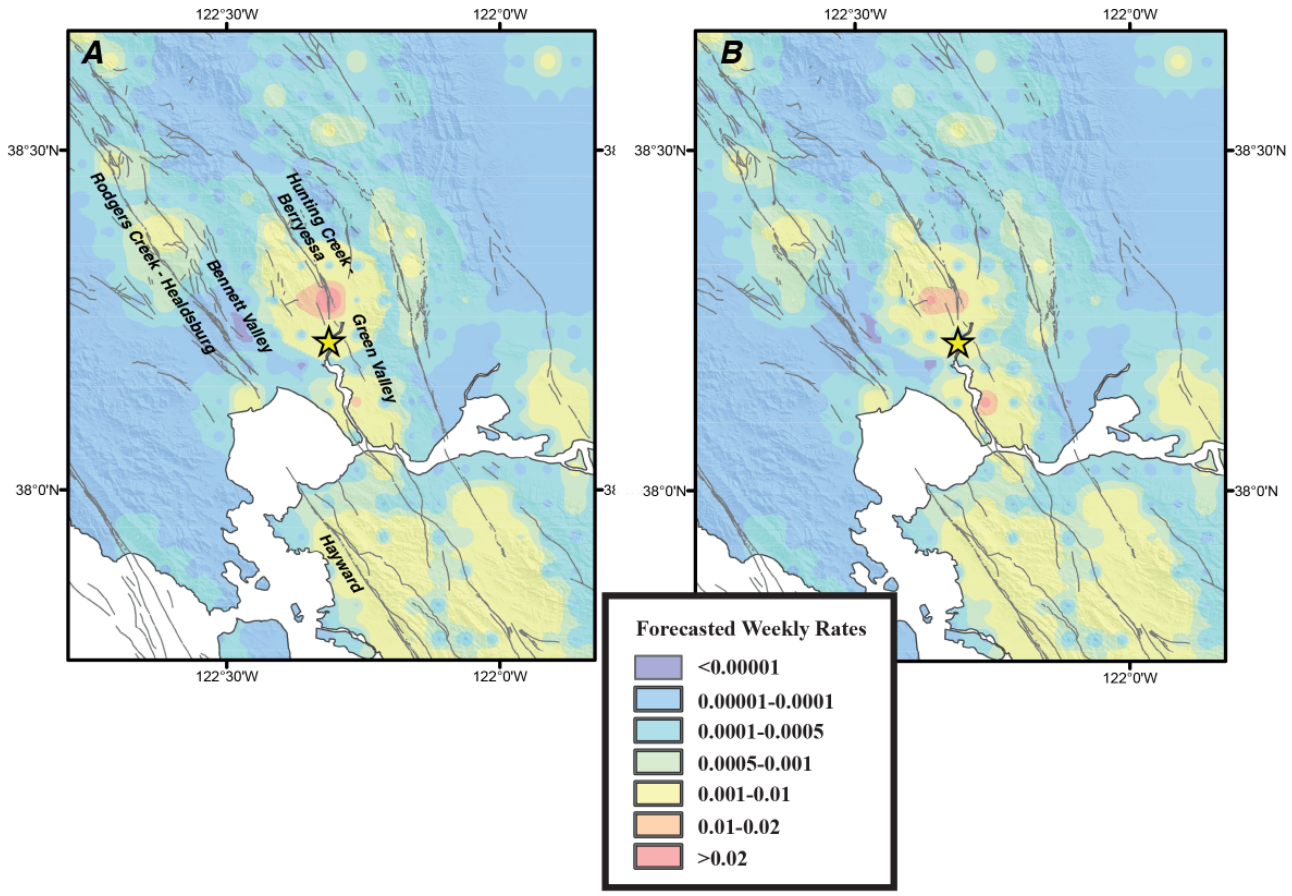

Figure 3. (a) Forecast first week of M≥3.0 seismicity rate density following the American Canyon earthquake based on Coulomb stresses calculated on a grid of optimally-oriented planes, and (b) a grid of faults with Hayward fault characteristics (strike=N34˚W, dip=90˚, rake=180˚).

3. Results

We summarize results of stress change calculations and predicted implications for future seismicity. The intention is to make these rapid forecasts, and then evaluate them over time by observing the evolution of seismicity. Formal California operational earthquake forecasting is currently under revision, but generally empirical/statistical methods are used [e.g., *Ogata*, 1988; 1998], though there may be some benefit to incorporating stress-based methods in tandem with empirical techniques [e.g., *Parsons and Segou*, 2014].

3.1 Results from Coulomb stress change mapping

The mapping in Figure 1 shows broad regions of calculated stress increases and decreases that affect major fault zones north of San Francisco Bay. In particular, we calculate a ~0.25 bar stress increase on the southern Rodgers Creek fault where it enters San Pablo Bay, and steps west onto the northern Hayward fault. Additionally, portions of the Green Valley fault also are calculated to have a ~0.25 bar increase; the Green Valley fault is the northern extent of the potentially linked Concord fault system that runs east of the San Francisco Bay area. We calculate a ~0.75 bar stress decrease on most of the West Napa fault. The simplified rupture model we used for the 2014 *M*=6.0 American Canyon earthquake means that we are unlikely to capture near-source aftershock activity very accurately, and this map should instead be interpreted for expected activity on adjacent faults.

3.2 Results from Coulomb stress changes resolved on UCERF3 faults

The spatial pattern of Coulomb stress changes resolved on individual faults in Figure 2 is comparable to the generalized mapping in Figure 1 because most of the major faults are parallel to the American Canyon earthquake source. We used a larger-area source model with an order of magnitude lower average slip, meaning that we calculate stress changes over a broader spatial extent, but with lower magnitudes in most places (Figure 2). We do note some additional effects; most importantly for hazard implications, we calculate a ~0.2 bar stress increase on the northern part of the Hayward fault, and a ~0.1 bar increase on the southern Rodgers Creek fault. We find a ~0.2 bar increase on parts of the Franklin and Green Valley faults, and a ~0.1 bar increase on the Contra Costa shear zone. Strong stress increases and decreases (between 1-2 bar) are

calculated on the West Napa fault, though uncertainty about the exact location of the mainshock rupture affects near-source stress calculations.

We calculate probability change on UCERF3 faults resulting from stress changes (Table 1). Using earthquake participation rates from *Field et al.* [2014] for each fault subsection (length equal to half the down-dip fault width), we find assumed nucleation recurrence intervals. Annual and 5-year time-dependent probability calculations are made for each subsection with and without stress interaction from the American Canyon event. Annual probability is generally low (< 1%) and not significantly different than Poisson because of the short duration [*Field and Jordan*, 2014], but is strongly affected (~10-50% changes) by stress changes (Table 1). Values are given for every subsection in Appendix 1.

UCERF3 Fault	**M_{min}**	**ΔCFF**	**1-year probability $M \geq M_{min}$**			**5-year probability $M \geq M_{min}$**		
		(bar)	**BPT**	**interaction**	**Δ (%)**	**BPT**	**interaction**	**Δ (%)**
Bennett Valley -	6.00	-0.17	0.09	0.04	-59	0.45	0.21	-55
Bennett Valley +	6.00	0.13	0.09	0.15	64	0.46	0.68	48
Concord	5.90	-0.10	0.30	0.20	-33	1.52	1.09	-29
Contra Costa Shear Zone (connector)	6.22	0.12	0.06	0.12	89	0.31	0.51	65
Franklin	6.25	0.21	0.06	0.15	141	0.32	0.59	89
Great Valley-Gordon Valley -	6.34	-0.10	0.06	0.04	-32	0.30	0.22	-28
Great Valley-Gordon Valley +	6.34	0.10	0.09	0.13	46	0.45	0.62	36
Great Valley Pittsburg-Kirby Hills	6.16	-0.10	0.16	0.11	-32	0.79	0.56	-28
Green Valley -	5.54	-0.26	0.36	0.17	-54	1.80	0.92	-50
Green Valley +	5.76	0.15	0.43	0.76	77	2.13	3.39	59
North Hayward -	6.04	-0.10	0.34	0.28	-18	1.68	1.43	-15
North Hayward +	6.12	0.16	0.30	0.48	62	1.48	2.17	47
Hunting Creek - Berryessa	5.86	-0.10	0.31	0.21	-33	1.56	1.12	-29
Los Medanos - Roe Island	6.69	-0.14	0.29	0.20	-33	1.47	1.05	-28
Rodgers Creek-Healdsburg -	6.18	-0.13	0.32	0.18	-44	1.59	0.97	-39
Rodgers Creek-Healdsburg +	6.17	0.13	0.30	0.50	65	1.52	2.27	49
West Napa -	6.30	-1.64	0.11	0.00	-99	0.55	0.01	-99
West Napa +	6.30	1.17	0.12	0.21	83	0.59	0.94	61

Table 1. Earthquake probability change values averaged across UCERF3 subsections; values are for $M \geq M_{min}$ as given for each fault. Average stress change values are given for each fault; if the fault has significant areas of positive and negative stress change, then the name is given with a "+" or "-" symbol respectively. "BPT" refers to time dependent probability using Brownian Passage Time distribution, whereas "interaction" includes the recurrence interval change and rate/state transient effects. "Δ" is the % probability change.

3.3 Results from Coulomb/rate-state aftershock forecasting

We make direct $M \geq 3.0$ aftershock forecasts based on Coulomb stress change mapping in Figure 3. The two calculations based on optimal vs. regionally aligned receiver faults are similar enough to discuss concurrently. We calculate that the highest expected weekly rate (≥0.02) of $M \geq 3.0$ earthquakes will be on the Green Valley fault northeast of the rupture zone (Figure 3). We also calculate relatively lower, but increased $M \geq 3.0$ rates above background (up to 0.01/week) on the Hayward, Rodgers Creek, and Bennett Valley faults. Rates calculated from stress-based methods tend to underpredict compared with observed values during the earliest phases of the aftershock period, primarily because reference background rates tend to be low, as the observation periods are not long enough to be fully representative [e.g., *Segou et al.*, 2013].

4. Conclusions

We forecast future seismicity from three stress-based methods for short (1 week) to intermediate (1-5 years) using information available within the first 24-hours after a mainshock. The purpose is to evaluate whether rapid, physics-based methods should have any role in operational forecasts. All three methods lead to similar conclusions. Earthquake rate increases are likely on parts of the Green Valley, Franklin, Contra Costa, southern Rodgers Creek, and northern Hayward faults as a result of the 24 August, 2014 M=6.0 American Canyon earthquake.

Earthquake rate decreases are also expected on parts of the Bennett Valley, Green Valley, Hayward and Rodgers Creek faults. We will evaluate these forecasts using observed seismicity rate changes, creep, and surface strain.

Acknowledgements We accessed the event page for the 24 August 2014 *M*=6.0 American Canyon earthquake at: http://earthquake.usgs.gov/earthquakes/eventpage/nc72282711#scientific for rapid CMT information from NCSS. We thank the editor at GRL and the reviewers.

References

Dawson, T. E. (2013), Appendix A - Updates to the California Reference Fault Parameter Database—Uniform California Earthquake Rupture Forecast, Version 3 Fault Models 3.1 and 3.2, USGS Open-File Report, v. 2013–1165, 66 pp., http://pubs.usgs.gov/of/2013/1165/pdf/ofr2013-1165_appendixA.pdf

Dieterich, J. (1994), A constitutive law for rate of earthquake production and its application to earthquake clustering, J. Geophys. Res., 99, 2601–2618.

Dieterich, J. H., and B. Kilgore (1996), Implications of fault constitutive properties for earthquake prediction, *Proc. Nat. Acad. of Sci. USA, 93*, 3787-3794.

Field, E. H., G. P. Biasi, P. Bird, T. E. Dawson, K. R. Felzer, D. D. Jackson, K. M. Johnson, T. H. Jordan, C. Madden, A. J. Michael, K. R. Milner, M. T. Page, T. Parsons, P. M. Powers, B. E. Shaw, W. R. Thatcher, R. J. Weldon, and Y. Zeng (2014), Uniform California Earthquake Rupture Forecast, Version 3 (UCERF3)—The time-independent model, Bulletin of the Seismological Society of America**,** 104, 1122–1180, doi: 10.1785/0120130164.

Field, E. H., and T. H. Jordan (2014). Time-Dependent renewal-model probabilities when date of last earthquake is unknown, Bull. Seism. Soc. Am, Submitted.

Hardebeck, J.L. and A.J. Michael (2004), Stress orientations at intermediate angles to the San Andreas fault, California, J. Geophys. Res., 109, B11303, doi: 10.1029/2004JB003239.

Matthews, M. V., W. L. Ellsworth, and P. A. Reasenberg (2002), A Brownian Model for Recurrent Earthquakes, Bull. Seismol. Soc. Am., 92, 2233 - 2250.

Ogata Y. (1988), Statistical models for earthquake occurrences and residual analysis for point processes, J. Amer. Statist. Assoc., 83, 9-27.

Ogata, Y. (1998), Space-time point-process models for earthquake occurrences, Ann. Inst. Stat. Math., 50, 379–402.

Okada, Y. (1992), Internal deformation due to shear and tensile faults in a half-space, Bull. Seismol. Soc. Am., 82, 1018-1040.

Parsons, T. (2002), Post-1906 stress recovery of the San Andreas fault system from 3-D finite element analysis, Journal of Geophysical Research, 107, 2162, doi:10.1029/2001JB001051

Parsons, T., Y. Ogata, J. Zhuang, and E. L. Geist (2012), Evaluation of static stress change forecasting with prospective and blind tests, Geophysical Journal International, v. 188, 1425–1440, doi: 10.1111/j.1365-246X.2011.05343.x.

Parsons, T., and M. Segou (2014), Stress, distance, magnitude, and clustering influences on the success or failure of an aftershock forecast: the 2013 M=6.6 Lushan Earthquake and other examples, Seismological Research Letters, v. 85, p. 44-51, doi: 10.1785/0220130100.

Segou, M., T. Parsons and W. Ellsworth (2013), Evaluation of combined physics based and statistical forecast models, Journal of Geophysical Research, v. 118, p. 6219–6240, doi:10.1002/2013JB010313.

Stein, R. S. (1999), The Role of Stress Transfer in Earthquake Occurrence, Nature, 402, 605-609.

Toda, S., R. S. Stein, P. A. Reasenberg, J. H. Dieterich, and A. Yoshida (1998), Stress transferred by the 1995 Mw=6.9 Kobe, Japan, shock: Effect on aftershocks and future earthquake probabilities, J. Geophys. Res., 103, 24,543-24,565.

Toda, S., Stein, R.S., Richards-Dinger, K., and S. Bozkurt (2005). Forecasting the evolution of seismicity in southern California: Animations built on earthquake stress transfer, J. Geophys. Res., 110, B05S16, doi:10.1029/2004JB003415

Wells, D. L., and K. J. Coppersmith (1994), New empirical relationships among magnitude, rupture length, rupture width, rupture area, and surface displacement, Bull. Seismol. Soc. Am., 84, 974– 1002, 1994.

WGCEP (2003), Earthquake Probabilities in the San Francisco Bay Region: 2002–2031, U. S. Geological Survey Open-File Report, 03-214, 235 pp.